

Energy size effects of two-dimensional Ising spin glasses

I. A. Campbell,¹ Alexander K. Hartmann,² and Helmut G. Katzgraber³

¹*Laboratoire des Verres, Université Montpellier II, 34095 Montpellier, France*

²*Institut für Theoretische Physik, Universität Göttingen, Tammannstraße 1, 37077 Göttingen, Germany*

³*Theoretische Physik, ETH Hönggerberg, CH-8093 Zürich, Switzerland*

(Dated: October 29, 2018)

We analyze exact ground-state energies of two-dimensional Ising spin glasses with either Gaussian or bimodal nearest-neighbor interactions for large system sizes and for three types of boundary conditions: free on both axes, periodic on both axes, and free on one axis and periodic on the other. We find accurate values for bulk-, edge-, and corner-site energies. Fits for the system with Gaussian bonds are excellent for all types of boundary conditions over the whole range of system sizes. In particular, the leading behavior for nonfree boundary conditions is governed by the stiffness exponent $\theta \approx -0.282$ describing the scaling of domain-wall and droplet excitations. For the system with a bimodal distribution of bonds the fit is good for free boundary conditions but worse for other geometries, particularly for periodic-free boundary conditions where there appear to be unorthodox corrections to scaling up to large sizes. Finally, by introducing hard bonds we test explicitly for the Gaussian case the relationship between domain walls and the standard scaling behavior.

PACS numbers: 75.50.Lk, 75.40.Mg, 05.50.+q

I. INTRODUCTION

The properties of the two-dimensional Edwards-Anderson Ising spin glass (ISG)^{1,2,3,4,5} with either Gaussian or bimodal ($\pm J$) nearest-neighbor interactions have been intensively studied. Efficient algorithms^{6,7,8} have been developed which provide exact ground-state energies and configurations for these systems up to large system sizes with $N = L \times L$ spins up to⁹ $L = 1800$, allowing for accurate measurements of fundamental parameters and stringent tests of theoretical predictions including precise evaluations of size-effect corrections to scaling.

In both Gaussian and bimodal disorder distributions, freezing occurs only at zero temperature,¹⁰ i.e. $T_c = 0$. For the Gaussian ISG as for any ISG system with a continuous distribution of interactions there is a unique ground state (together with its reversed image). At $T = 0$ the thermodynamic limit correlation function $G(r)$ is constant, $G(r) = 1$ for all distances r . As the critical exponent η is defined through $G(r) \sim r^{-(d-2+\eta)}$ at the ordering temperature, $\eta = 0$. For the $\pm J$ ISG, the ground state is highly degenerate, with a residual entropy at zero temperature¹¹ $S(T = 0) = 0.078(5)k_B$. In consequence the time averaged correlation function $G(r)$ drops with increasing r , meaning η must be positive.¹² The domain-wall stiffness has been measured accurately through comparisons of the energies of samples with periodic and antiperiodic boundary conditions in one direction. For the Gaussian ISG, $\theta = -0.282(2)$.^{10,13} From the scaling rules applied at a zero temperature transition,^{14,15} we obtain for the critical exponent $\nu = -1/\theta$, hence $\nu = 3.55(3)$.^{15,16} For the $\pm J$ 2d ISG, large- L simulations¹⁰ on samples with periodic/antiperiodic boundary conditions along one axis and free boundary conditions on the other axis showed $\theta = 0$, with significant corrections to scaling up to $L \sim 100$. Finite-size scaling and Migdal-Kadanoff simulations on a variety of 2d ISG samples with different

distributions of interactions are consistent with a unique lower critical dimension $d_l \sim 2.5$; for all the samples with discrete distributions of interactions $\theta = 0$ at all dimensions below the lower critical dimension.¹⁷ For these systems the effective exponent ν is infinite. The correlation length diverges exponentially¹² and the specific heat drops to zero as $\exp(-n\beta)$; data were analyzed using n equal to^{18,19} 4 but recent work²⁰ is consistent with $n = 2$. Although we will be concerned here only with zero-temperature behavior, we can note that there have been conflicting estimates of the “droplet” excitation exponent for the Gaussian ISG, which standard arguments indicate should be identical to θ . It has been suggested that apparent disagreements are artifacts due to corrections to scaling²¹ but Berthier and Young found²² that whether such corrections are visible seems to depend on the details of the measurements.

We have carried out measurements of the ground-state energy per spin on square samples as a function of system size L for three different types of boundary condition: free along both x and y pairs of boundaries (to be referred to as ffbc), free along one pair of boundaries and periodic along the other pair to give a cylindrical geometry (pfbc), and periodic along both pairs of boundaries to give a toroidal geometry (ppbc). These three geometries are physically distinct. In the ffbc case, there are bulk sites, edge sites, and corner sites. However the system has no boundary condition constraints, or in other words it can be taken to contain no “domain walls,” at least for a sample with a unique ground state. In the pfbc scenario there are edge sites but no corner sites; on the other hand the sample is constrained by the boundary condition along one direction. Finally for the familiar ppbc case there are no edges or corners but there are constraints along both directions. It is for this geometry with no boundaries that the standard scaling approach should apply.

The behavior of the fbc systems can be explained in simple geometrical terms. The behavior of the Gaussian systems with pfbc and ppbc is governed by an algebraic term with the exponent $\theta \approx -0.282$, the same value as the exponent describing the behavior of domain-wall and droplet excitations.^{23,24} For this reason, we also compare sample by sample fbc and pfbc realizations with the same interaction set and look for the appearance of system-spanning domain walls. Finally, we introduce *hard bonds* to force system-spanning domain walls and study how the appearance of these depends on the fraction of hard bonds.

The paper is organized as follows: In Sec. II we introduce the model, observables, and details of the algorithms used. Scaling arguments are summarized in Sec. III. Results for the fbc, ppbc, and pfbc scenarios are presented in Secs. IV, V, and VI, respectively. Domain-wall calculations are discussed in Sec. VII and concluding remarks are contained in Sec. VIII.

II. MODEL AND ALGORITHMS

The Hamiltonian of the two-dimensional Ising spin glass is given by

$$\mathcal{H} = - \sum_{\langle i,j \rangle} J_{ij} S_i S_j, \quad (1)$$

where the sites i lie on a square lattice in two dimensions and the J_{ij} are nearest-neighbor interactions. In the Gaussian case the couplings are chosen according to a Gaussian distribution with zero mean and standard deviation unity, whereas in the bimodal case the couplings J_{ij} can take values of $\{\pm 1\}$ with equal probability.

In greater than two dimensions, or in the presence of a magnetic field, the exact calculation of spin-glass ground states belongs to the class of NP -hard problems.^{25,26} This means that only algorithms with exponentially increasing running times are known. Here, we have studied mainly square lattices with periodic boundary conditions in at most one direction without external magnetic fields. For this special case of a planar system there are efficient polynomial-time “matching” algorithms.⁶ The basic idea is to represent each realization of the disorder by its frustrated plaquettes.²⁷ Pairs of frustrated plaquettes are connected by paths in the lattice and the weight of a path is defined by the sum of the absolute values of the coupling constants which are crossed by the path. A ground state corresponds to the set of paths with minimum total weight, such that each frustrated plaquette is connected to exactly one other frustrated plaquette. This is called a minimum-weight perfect matching. The bonds which are crossed by paths connecting the frustrated plaquettes are unsatisfied in the ground state, and all other bonds are satisfied.

For the calculation of the minimum-weight perfect matching, efficient polynomial-time algorithms are

TABLE I: The number of samples for the ground-state calculations for different system sizes, distributions and free-free (fbc), resp., free-periodic (pfbc) boundary conditions.

L	Gaussian fbc	Gaussian pfbc	$\pm J$ fbc	$\pm J$ pfbc
2	1×10^6		4×10^6	
3	1×10^6	1×10^6	1×10^6	1×10^6
4	9.1×10^5	1×10^6	1×10^6	9.4×10^5
6	5.1×10^5	9.9×10^4	5×10^5	5.4×10^5
8	2.1×10^5	9.9×10^4	2×10^5	3.4×10^5
10	1.1×10^5	9.9×10^4	1×10^5	1.4×10^5
16	4×10^4	9.9×10^4	1×10^4	4×10^4
20	1×10^4	1×10^4	1×10^4	4×10^4
30	1×10^4	1×10^4	1×10^4	4×10^4
40	1×10^4	1×10^4	1×10^4	3.9×10^4
60	1×10^4	1×10^4	1×10^4	4×10^4
80	1×10^4	1×10^4	1×10^4	4×10^4
120	1×10^4	1×10^4	1×10^4	4×10^4
160	1×10^4	1.1×10^4	1×10^4	4×10^4
240	724	2800	5×10^5	4.6×10^4
320		3710	5×10^5	2.4×10^4
480				2×10^4

available.^{7,8} Recently, an implementation has been presented,⁹ where ground-state energies of large systems of size $N \leq 1800^2$ were calculated. Here, an algorithm from the LEDA library²⁸ has been applied, which limits the system sizes due to the restricted size of the main memory of the computers which we used.

Furthermore, we have studied two-dimensional systems with fully periodic boundary conditions. Here, we use the spin-glass ground-state server at the University of Cologne²⁹ where a “branch-and-cut” method^{30,31} (see Ref. 32 for a tutorial on optimization problems and techniques, including branch-and-bound and branch-and-cut) is used, which is currently the fastest exact algorithm for computing spin-glass ground states,³³ with the exception of the polynomial-time special cases mentioned above. Nevertheless, the CPU time increases faster than a power of the system size. Therefore we cannot study as large systems as are possible with the matching algorithm. Nonetheless, the implementation of the branch-and-cut algorithm on the Cologne server is very efficient, hence we can still study quite a large range of sizes, in practice $L \leq 64$.

The numbers of samples over which averages are taken are shown in Tables I and II.

III. SCALING

We want to find the size-dependence of the energy from simple scaling arguments for the generic ppbc case and follow closely along the lines of the scaling discussion presented in Ref. 14. The internal energy per spin e of a

TABLE II: The number of samples for the ground-state calculations for full periodic (ppbc) boundary conditions, for different system sizes and disorder distributions.

L	Gaussian	$\pm J$
3	5×10^4	1×10^4
4	2×10^4	1×10^4
6	1×10^4	5×10^3
8	1×10^4	5×10^3
12	5×10^3	2×10^3
16	1×10^3	2×10^3
24		2×10^3
32	2×10^3	2×10^3
64	1×10^3	

thermodynamic system can be expressed as a derivative of the free energy per spin f with respect to the temperature:

$$e = -\frac{1}{\beta^2} \frac{d(\beta f)}{dT}, \quad (2)$$

where $\beta = 1/T$, T the temperature.

We assume that the scaling of the temperature dependence of the correlation length is $\xi \sim (T - T_c)^{-\nu}$ or $(T - T_c) \sim \xi^{-1/\nu}$. Therefore

$$dT \sim \xi^{-(1+1/\nu)} d\xi. \quad (3)$$

Hence, we obtain

$$e(T) = -\frac{1}{\beta^2} \frac{d(\beta f)}{d\xi} \frac{d\xi}{dT} + B(T). \quad (4)$$

$B(T)$ is the smooth noncritical background.

Using basic finite-size scaling arguments,³⁴ we know that for the singular part of the free energy $\beta f \sim \xi^{-d}$.³⁵

First we discuss the case $T_c > 0$. In this case the factor $1/\beta^2$ is not critical. Therefore we obtain

$$e(T) \sim \frac{1}{\beta_c^2} \xi^{-(d-1/\nu)} + B(T), \quad (5)$$

where $\beta_c = 1/T_c$. At T_c , $\xi_L = \mathcal{C}_1 L$, \mathcal{C}_1 a constant, so the critical behavior of e_L is

$$e_L - e_\infty \sim L^{-(d-1/\nu)} \quad (T_c > 0). \quad (6)$$

Next, we discuss the case $T_c = 0$. Now β is critical, $\beta \sim \xi^{1/\nu}$, hence

$$e \sim \frac{1}{\xi^{2/\nu}} \xi^{-(d-1/\nu)} + B = \xi^{-(d+1/\nu)} + B. \quad (7)$$

For a finite system of size L ,

$$e_L - e_\infty \sim L^{-(d+1/\nu)} \quad (T_c = 0). \quad (8)$$

For $T_c = 0$ one also has the scaling relation³⁶ between the domain-wall stiffness exponent θ and the exponent ν , $\theta = -1/\nu$, therefore

$$e_L - e_\infty \sim L^{-(d-\theta)} \quad (T_c = 0). \quad (9)$$

For the $\pm J$ case, $T_c = 0$ and the correlation length diverges exponentially. Following through the algebra with¹² $\xi = \exp(2/\beta)$ leads to $e_L - e_\infty \sim L^{-d}$, which is just the same as Eq. (9) with $\theta = 0$, corresponding to $\nu = \infty$.

Equation (8) is a scaling identity for any system with ppbc and $T_c = 0$, and there is no need to appeal to specific physical arguments to justify it. Any deviations from this identity must be due to corrections to scaling. (We can note that Bouchaud *et al.*³⁷ refer to this scaling term as the ‘‘correction to scaling.’’)

The leading correction to scaling should be either a renormalization group theory (RGT) irrelevant operator correction giving the form

$$e_L - e_\infty \sim L^{-(d-\theta)}(1 + \mathcal{K}_1 L^{-\omega} + \dots) \quad (10)$$

where ω is the RGT leading correction to scaling exponent and \mathcal{K}_1 is a constant, or an analytic correction which plausibly introduces a term $\mathcal{K}_2 L^{-2}$.^{38,39} This ‘‘analytic’’ term is unrelated to the RGT irrelevant operators. The arguments leading to a prediction for the energy correction at this level can be very involved, even for the canonical $2d$ Ising ferromagnet where there is no irrelevant operator term but there are analytic terms in odd powers of $1/L$.^{38,39,40} For ISGs the leading term in the RGT ϵ -expansion for $\omega(d)$ as a function of dimension d is⁴¹: $\omega(d) = (6-d) + \dots$; as we can safely assume that by $d = 2$, $\theta + \omega \gg 2$ hence the dominating correction term is an analytic term.

Thus finally, for ppbc from standard scaling arguments we expect

$$e_L = e_\infty + \mathcal{L}_1 L^{-(d-\theta)} + \mathcal{L}_2 L^{-2} + \dots, \quad (11)$$

where the \mathcal{L}_1 term is the scaling term and the \mathcal{L}_2 term is the analytic correction term. In practice, if θ is small compared to d , it will be hard to distinguish between this sum of two terms and an ‘‘effective’’ scaling,

$$e_L = e_\infty + \mathcal{L}_{\text{eff}} L^{-(d-\theta_{\text{eff}})}, \quad (12)$$

with a single effective exponent θ_{eff} whose value is a function of $\mathcal{L}_2/\mathcal{L}_1$ and which can be larger or smaller than θ depending on the sign of this ratio.

Although the remark is irrelevant for the two-dimensional case, we can note that if $T_c > 0$ this discussion is valid *mutatis mutandi* at T_c ; however if $T_c > 0$ scaling rules do not apply below T_c and in particular at $T = 0$. Alternative physical arguments must be used for discussing the ground-state behavior.

IV. FREE BOUNDARY CONDITIONS (FFBC)

If boundary conditions are free along all four edges we can consider that there are no external constraints on the system. There are however edge and corner sites, edge bonds and corner bonds. The total number of bonds is equal to $2(L^2 - L)$ while the number of spins is L^2 , hence we present a discussion in terms of the energy per spin e_L or alternatively twice the energy per bond $2e_L^{\text{bond}}$ (the values will become identical in the infinite L limit).

A heuristic geometrical scaling consists in writing twice the energy per bond as

$$2e_L^{\text{bond}} = \mathcal{A}^* + \mathcal{B}^*/L + \mathcal{C}^*/L^2, \quad (13)$$

where \mathcal{A}^* , \mathcal{B}^* , and \mathcal{C}^* are constants. Physically the first term in Eq. (13) represents the energy per bulk bond, the second term is a correction for the energy difference between an edge and a bulk bond, and the third term a further correction for a corner bond. Even if the localization of the energy differences onto the edge or corner bonds is only approximate so the identification between terms and bonds is not rigorous, on geometrical grounds the ffbc energy size effects can be expected to have strictly this form with no further terms, at least down to small L values where neighboring corner effects begin to interfere. Translating Eq. (13) into terms of energy per spin, i.e. using $E_L = (L^2 - L)e_L^{\text{bond}} = L^2e_L$, gives an energy per spin,

$$e_L = \mathcal{A}^* - (\mathcal{A}^* - \mathcal{B}^*)/L - (\mathcal{B}^* - \mathcal{C}^*)/L^2 - \mathcal{C}^*/L^3. \quad (14)$$

For the isolated spin ($L = 1$) the energy per bond is not defined, but the energy per spin is identically zero. By inspection Eq. (14) happens to have a form such that e_L must be exactly equal to zero for $L = 1$. We can also write

$$e_L = \mathcal{A} + \mathcal{B}/L + \mathcal{C}/L^2 + \mathcal{D}/L^3, \quad (15)$$

with $\mathcal{A} = \mathcal{A}^*$, $\mathcal{B} = -(\mathcal{A}^* - \mathcal{B}^*)$, $\mathcal{C} = -(\mathcal{B}^* - \mathcal{C}^*)$, and $\mathcal{D} = -\mathcal{C}^*$. For the Gaussian ffbc data the fit to Eq. (15) is shown in Fig. 1. It can be seen that for the entire range of sizes from $L = 1$ to $L = 240$ the three-parameter fit is excellent with $\chi^2 = 0.67$. The same data with the same fit parameters \mathcal{A} , \mathcal{B} , \mathcal{C} , and \mathcal{D} are presented as a difference plot, i.e. as the difference between the fit and the actual data, in the inset of Fig. 1. Remarkably, this naive equation with three free parameters is in agreement with the measurements to within one or two parts in 10^4 for the whole range of L from $L = 240$ down to and including $L = 1$. The fit parameters are given in Table III.

If we repeat the same analysis for $\pm J$ bonds, using data from $L = 4$ to $L = 320$, the agreement is almost equally good, cf. Fig. 2. The fit parameters ($\chi^2 = 1.29$) are given in the Table III. (We have not included in the fit the point for $L = 2$ which lies almost 3% above the trend. By this size each system has only four bonds and

TABLE III: Fit parameters according to Eq. (14) for ff boundary conditions, as well as for Gaussian and bimodal distributed disorder.

parameter	Gaussian	$\pm J$
\mathcal{A}^*	-1.31479(2)	-1.40197(2)
\mathcal{B}^*	-0.3205(9)	-0.5492(20)
\mathcal{C}^*	0.042(3)	0.506(18)

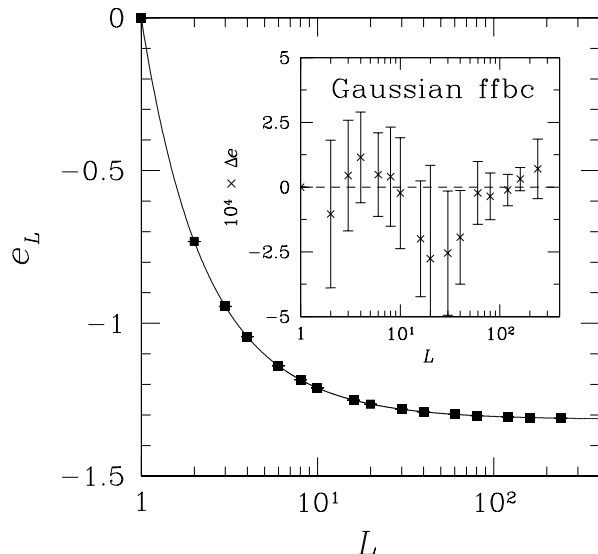


FIG. 1: Energy per spin for the ffbc Gaussian case. The solid line represents a three-parameter fit to Eq. (14) with $\chi^2 = 0.67$. The inset shows the difference between the fit and the actual data, Δe , represented as an energy per spin. Fit parameters are summarized in Table III.

there are only five possible energies for any $\pm J$ system. As one might foresee, quantization effects seem to break down the precise scaling by this size.)

The fit extrapolates to a bulk (or infinite lattice size) energy per spin of

$$e_{\text{bulk}}^{\text{Gauss}} = -1.31479(2), \quad (16)$$

for the Gaussian case. The most recent published value is $e_{\text{bulk}}^{\text{Gauss}} = -1.317(1)^{30}$. For the $\pm J$ case the present data give a bulk energy per spin of

$$e_{\text{bulk}}^{\pm J} = -1.40197(2). \quad (17)$$

This estimate is compatible with the very precise published value $e_{\text{bulk}}^{\pm J} = -1.401938(2)^9$. Notice that the bulk energy of the bimodal system is significantly more negative than the bulk energy of the Gaussian system.

In the ffbc lattice with L^2 spins there are $(L - 2)^2$ bulk sites, $4L - 8$ edge sites, and 4 corner sites. We associate energies e_{bulk} , e_{edge} , and e_{corner} with sites at each of these positions, respectively (equal to half the sum of the adjacent bond energies). Using $E_L = L^2e_L =$

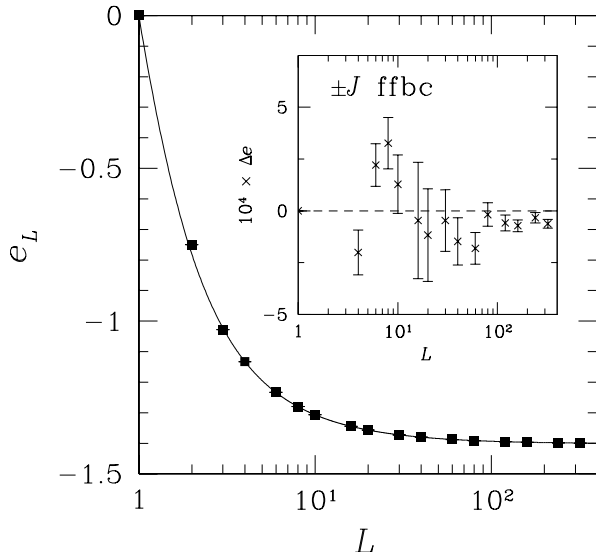


FIG. 2: Energy per bond for the ffbc $\pm J$ case. The solid line corresponds to a three-parameter fit to Eq. (14) with $\chi^2 = 1.29$. The inset shows the difference between the fit and the actual data. Fit parameters are summarized in Table III.

$(L-2)^2 e_{\text{bulk}} + (4L-8)e_{\text{edge}} + 4e_{\text{corner}}$ and comparing with Eq. (15), we can make the identifications for the energies per site,

$$\begin{aligned} e_{\text{bulk}} &= \mathcal{A}, \\ e_{\text{edge}} &= \mathcal{A} + \mathcal{B}/4, \\ e_{\text{corner}} &= \mathcal{A} + \mathcal{B}/2 + \mathcal{C}/4. \end{aligned} \quad (18)$$

Because each bulk site has four bonds, each edge site three bonds, and each corner site two bonds, and because each bond is shared with a neighbor site, to obtain the average bond energies for the bonds linking to these three types of sites we divide e_{bulk} , e_{edge} , e_{corner} by 2, 1.5, and 1, respectively.

The bulk, edge, and corner energies per bond evaluated according to Eq. (18) when inserting the measured scaling parameters \mathcal{A} , \mathcal{B} , and \mathcal{C} are shown in Table IV. As is to be expected in both cases the edge and corner energies are more negative than the bulk bond energies because the bonds at the edges and corners are less frustrated. The de-frustration effects can be seen to be $\sim 50\%$ stronger in the $\pm J$ case as compared to the system with Gaussian interactions.

The Gaussian values can be compared with explicit bond-by-bond sample-by-sample measurements of bulk, edge, and corner bond energies. Averaging over 100 $L = 100$ ground states with Gaussian bonds we obtain $-0.6576(4)$, $-0.698(2)$, and $-0.66(2)$ for the mean local bulk, edge and corner bond energies, respectively. These values are compatible with the more precise values estimated by scaling, allowing for the fact that the definitions are identical for the bulk bonds but not for the edge or corner bonds. In these cases the scaling values implic-

TABLE IV: Energy per bond for ff boundary conditions. The edge and corner energies are larger in magnitude than the bulk values because the bonds at the edges and corners are less frustrated.

bond	Gaussian	$\pm J$
Bulk	$-0.65740(1)$	$-0.70099(1)$
Edge	$-0.7108(2)$	$-0.7925(4)$
Corner	$-0.727(1)$	$-0.821(4)$

itly include energy changes at slightly perturbed further bonds.

V. PERIODIC-PERIODIC BOUNDARY CONDITIONS (PPBC)

Periodic-periodic boundary conditions are the standard geometry in which simulations are conventionally carried out, and to which the critical scaling rules discussed in Sec. III [Eq. (8)] should apply. There are no edges or corners and all sites are on average in equivalent environments. The infinite-size limit energy per spin should be identical to the infinite size bulk energy per spin in the ffbc geometry.

For the Gaussian case, high precision domain-wall measurements give excellent scaling with an exponent $\theta = -0.282(2)$,^{10,13} and we should expect

$$e_L - e_\infty \sim L^{-(2-\theta)}, \quad (19)$$

up to correction terms. In fact we go further and test much more stringent assumptions: first, that corrections are negligible, and second that the energy per spin at large and moderate L extrapolates exactly to $e_L = 0$ at $L = 1$. Thus we test the relation

$$e_L = e_\infty \left[1 - L^{-(2-\theta)} \right]. \quad (20)$$

Here we have no free parameters as we adopt the value $e_\infty = -1.31479$ obtained above in the ffbc measurement, and the value $\theta = -0.282$ obtained from domain-wall measurements. We exclude $L = 2$ as this size is pathological in ppbc because of wrap-around effects for the interactions. For the “fit” $\chi^2 = 0.92$ for sizes from $L = 3$ to 64. The data are represented in Fig. 3 with a difference plot in the inset. It can be seen that this parameter-free expression represents the high precision data to within the statistical accuracy. Alternatively, assuming that the e_∞ value is correct and that there are no corrections to scaling, we can fit leaving θ as a free parameter. We obtain a best fit for the stiffness exponent,

$$\theta = -0.281(7), \quad (21)$$

i.e., $\nu \approx 3.55$, with $\chi^2 = 0.78$. This is an accurate independent value in excellent agreement with the domain-wall estimates, as well as finite-temperature

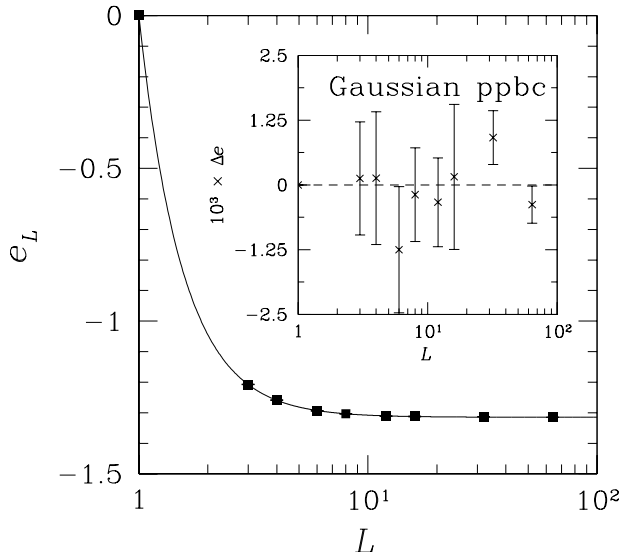


FIG. 3: Energy for the ppbc Gaussian case. The solid line corresponds to a “fit” with *no free parameters* to Eq. (20) which yields a quality of fit $\chi^2 = 0.92$. The inset shows the difference between the fit and the actual data.

estimates.^{15,16} The assumptions that we have made are either exact or are very good approximations.

For the $\pm J$ case (Fig. 4) the situation is less clear cut. If we make the same stringent parameter-free assumptions, taking $e_\infty = -1.401938$ and $\theta = 0$ we obtain a rather mediocre fit, $\chi^2 \approx 15$ for the data from $L = 3$ to $L = 32$ or $\chi^2 \approx 6.5$ for the data from $L = 4$ to $L = 32$. Relaxing the condition $e_{L=1} = 0$ gives a better fit, $e_L = e_\infty + 1.319/L^2$ with $\chi^2 \approx 2.6$ for $L = 4$ to $L = 32$. This could be understood as an analytic correction term appearing. Such a term should be expected to also have the form L^{-2} and so in the $\pm J$ case where $\theta = 0$ it would simply modify the prefactor of the scaling term which is also proportional to L^{-2} . Alternatively, if we assume that for the range of L over which the energy differences can be measured the *effective* value of θ is different from zero, i.e., when incorporating the corrections to scaling into it, we can fit to Eq. (20) with θ as a free parameter. The best fit in this case from $L = 4$ to $L = 32$ corresponds to $\theta = -0.04(1)$, with $\chi^2 \approx 2.0$. This discussion indicates that the strict zero free parameter scaling that gives virtually perfect agreement in the Gaussian case explains the form of e_L to much lower precision in $\pm J$ case. This could mean that unknown higher-order corrections to scaling must be taken into account to represent the behavior also at the relatively small sizes accessible for the ppbc case. We believe that this behavior is due to the discreteness of the bond distribution, leading to a high ground-state degeneracy of the $\pm J$ model; see the discussion at the end of the next section.

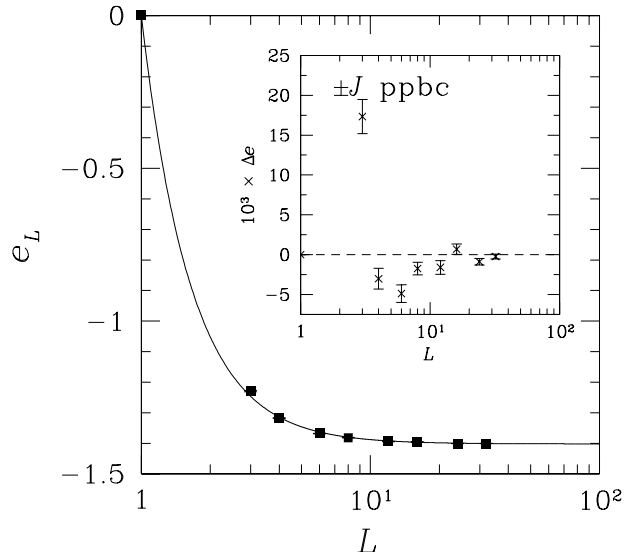


FIG. 4: Energy for the ppbc $\pm J$ case. The solid line corresponds to a parameter-free “fit” according to Eq. (20) with $e_\infty = -1.401938$ and $\theta = 0$. The inset shows the differences between the fit and the actual data.

VI. PERIODIC-FREE BOUNDARY CONDITIONS (PFBC)

We study a cylindrical geometry where the boundary conditions are free along one pair of edges, and periodic for the perpendicular pair. In the large- L limit the bulk site or bond energy term per spin or per bond should again be exactly the same as in the fbbc case. We assume that the free-edge size effect per edge site also has the same value as in the fbbc case. There are no corners. Because the periodic boundary condition imposes a constraint, *a priori* one can also expect terms of the same type as in ppbc. The edge effects being allowed for, we assume that the scaling term is again proportional to $L^{-(2-\theta)}$ and we allow for an analytical correction term proportional to L^{-2} . The total number of bonds is $2L^2 - L$. Following the same arguments as in the fbbc case presented in Sec. IV we test the expression

$$e_L = \mathcal{A}^* + \frac{1}{2L}(\mathcal{B}^* - \mathcal{A}^*) - \frac{1}{4L^2}\mathcal{B}^* + \mathcal{L}_1 L^{-(2-\theta)} + \frac{\mathcal{L}_2}{L^2}, \quad (22)$$

where \mathcal{A}^* and \mathcal{B}^* are taken directly from the fbbc analysis, so we have only two free parameters for the fit.

For the Gaussian pfbc data, the fit to points from $L = 3$ to $L = 320$ is excellent, $\chi^2 = 0.26$ for $\mathcal{L}_1 = 1.019(9)$ and $\mathcal{L}_2 = -0.203(7)$. The data are shown in Fig. 5. If there is no L^{-2} correction term, the fit is significantly worse. We note that for the pfbc geometry an analytical correction term is necessary, and that the fit does not extrapolate exactly to $e_L = 0$ at $L = 1$. The fit is thus less aesthetically pleasing than was the case for either fbbc or the ppbc cases; we can conclude that nevertheless a high quality consistent analysis can be made of the pfbc

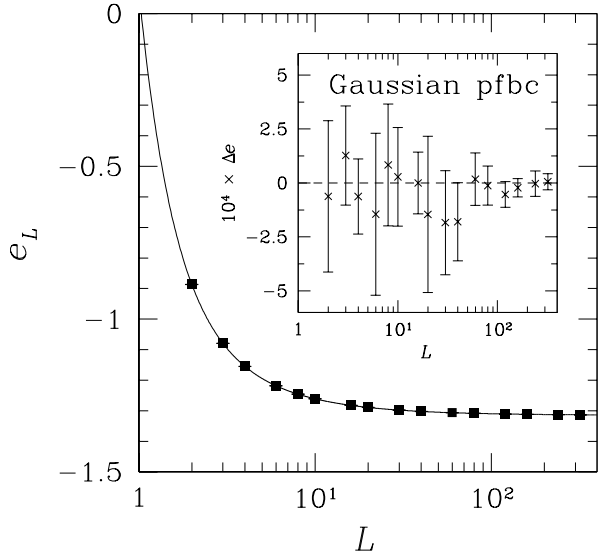


FIG. 5: Energy for the pfbc Gaussian case and fit to Eq. (22) (see the text). The inset shows the differences between the fit and the actual data.

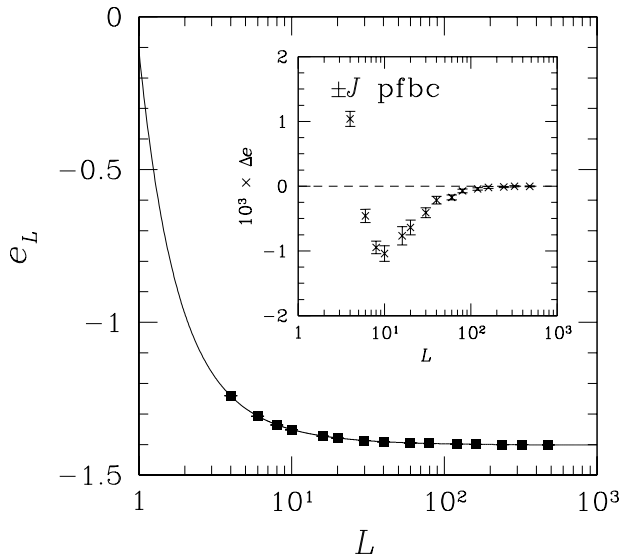


FIG. 6: Energy for the pfbc $\pm J$ case and fit to Eq. (22) (see the text). The inset shows the differences between the fit and the actual data.

Gaussian data over the entire range of L using physically reasonable assumptions for the fits. However, it is not clear to us why an analytic correction term is needed for the pfbc geometry while the ppbc fit is excellent without any such correction.

For the $\pm J$ data, see Fig. 6, we proceed in exactly the same way. In this case the large- L stiffness exponent¹⁰ $\theta = 0$, so one should expect both the scaling and the analytical correction to contribute to a single composite term in L^{-2} . With this assumption the fit to the pfbc

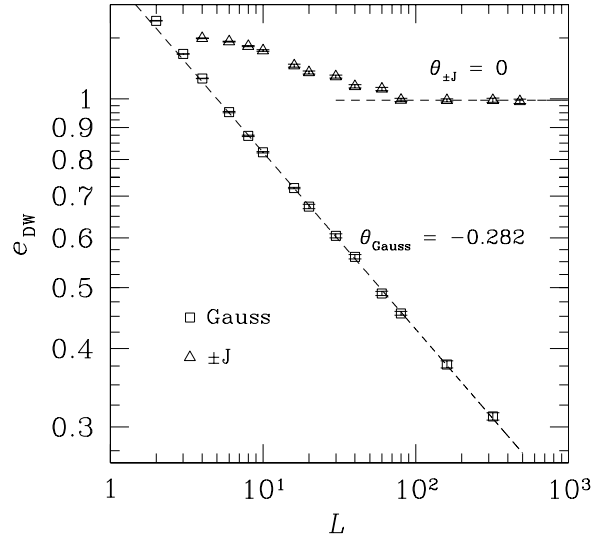


FIG. 7: Domain-wall energies for Gaussian as well as $\pm J$ bonds. While in the Gaussian case the asymptotic power-law behavior appears for small system sizes, in the $\pm J$ case the asymptotic behavior where $\theta = 0$ does not appear until lattice sizes $L \approx 100$.

data from $L = 3$ to $L = 480$ is very poor ($\chi^2 \approx 30$).

To understand this behavior, we can note that the domain-wall stiffness measurements¹⁰ on the $\pm J$ ISG taken in the same pfbc conditions show strong and nonorthodox corrections to scaling which extend to $L \sim 100$; the data only attain the limiting behavior $\theta = 0$ for very large L , as can be seen in Fig. 7. In the Gaussian case both the domain-wall stiffness and the size dependence of the energy in the pfbc geometry follow consistently the expected scaling rules. For the $\pm J$ case in pfbc geometry on the other hand corrections to scaling of the standard form are not adequate to explain the deviations from scaling which exist up to large values of L . This is probably due to the discreteness of the interactions for the $\pm J$ case. This discreteness leads to a high degeneracy, which in turn allows in two dimensions to form domain-walls with almost no energy (as for the Gaussian case). But considerably larger system sizes have to be studied to find these low-energy paths, because, in contrast to the Gaussian case, there are no bonds which can be broken at the cost of very small energies. Every broken bond costs an energy $2J$. Indeed, by introducing possible zero bonds, i.e., treating a diluted system, the effect is reduced.¹⁷ As we will show in the next section, the scaling of the ground-state energy is related to the physical appearance of domain-walls, hence the same unorthodox and strong corrections are to be expected for the $\pm J$ case.

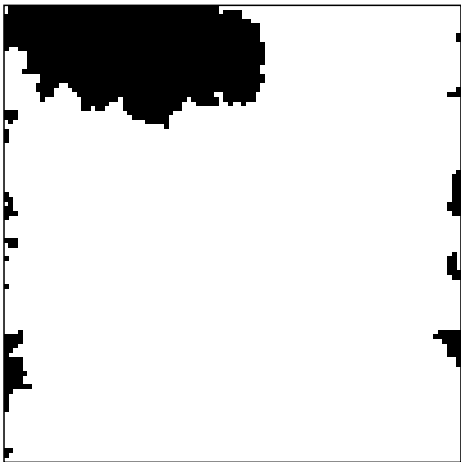


FIG. 8: Difference between the ground states of one realization ($L = 100$) for free and periodic boundary conditions in the x -direction. Bonds are changed along the vertical axes.

VII. APPEARANCE OF DOMAIN WALLS

We have seen, in particular for the model with a Gaussian distribution of the interactions, that for free boundary conditions the size dependence of the ground-state energy can be explained by simple algebraic terms. As soon as periodic boundary conditions are applied, a term $\sim L^{-(d-\theta)}$ appears, θ being the exponent describing the size-dependence of the energy of elementary excitations such as droplets or domain walls. In this section we want to therefore test whether really the occurrence of domain walls, induced by the boundary conditions, is responsible for this scaling. For this purpose, we study systems with Gaussian interactions and fbc, calculate the ground state, then we change the boundary conditions to pbc (by adding one column of random bonds wrapping around the system), recalculate the ground state, and compare the two different ground states. In Fig. 8 the result for one sample of size $L = 100$ is shown. The result is typical: no system-spanning domain walls are obtained, but a collection of smaller and few larger droplet-like excitations pinned to the boundary. We observe that quite often the larger droplets span even larger fractions of the systems.

To test whether system-spanning domain walls play a role in this framework, we perform the following simulation: We start with fbc, calculate the ground state, and then switch to pbc. Now a fraction p of the bonds which wrap around the system is chosen as *inverted hard bonds*. This means that they have a very large magnitude, such that they are satisfied in any ground state. The sign is chosen in a way such that it forces the two adjacent spins to take opposite relative orientations with respect to the fbc ground state, i.e. exactly one spin flips. This means, the inverted hard bonds force a domain wall into the system at this position. The remaining fraction $(1 - p)$ of the additional bonds is again chosen from a Gaussian dis-

TABLE V: Number of samples for the ground-state calculations for the samples (Gaussian distribution of the bonds) having first full free, then free boundary conditions in the y -direction and mixed random-weak/inverted-hard boundary conditions in the x -direction (with a fraction p of the boundary bonds being inverted hard), for different system sizes L and values of p . For the different values of $p > 0$, always the same number of samples are taken for a fixed size, except for the largest size $L = 160$.

L	$p = 0$	$p > 0$
6	21000	1000
10	21000	1000
16	20000	
20	10000	1000
30	20000	
40	20000	1000
60	15000	
80	13000	1000
120	15000	
160	15250	700-4600

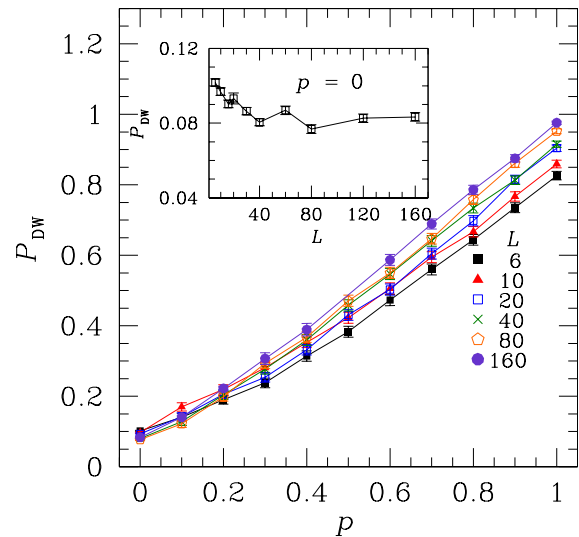


FIG. 9: (Color online) Probability P_{DW} of the occurrence of a system-spanning domain wall as a function of the fraction p of inverted hard bonds wrapping around the system, for different system sizes L . The lines connect the dots and are guides to the eye only. The inset shows $P_{\text{DW}}(p = 0)$ as a function of L . We see that for $p = 0$ in average only $\sim 10\%$ of the domain walls are system spanning.

tribution with zero mean and standard deviation unity. The number of samples studied as a function of L and p are shown in Table V.

In Fig. 9 the probability P_{DW} that a domain wall spans from the top to the bottom is shown as a function of p . Clearly, P_{DW} increases with growing p and reaches unity for largest system sizes when $p \rightarrow 1$, as expected. For

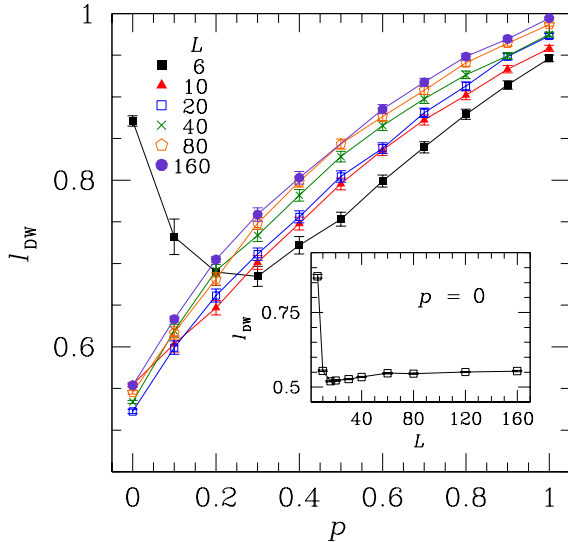


FIG. 10: (Color online) Length l_{DW} (in units of L along the y -direction) of the longest nontrivial domain wall as a function of the fraction p of inverted hard bonds wrapping around the system, for different system sizes L . Lines are guides to the eyes only. The inset shows $l_{\text{DW}}(p = 0)$ as a function of L .

large p , l_{DW} grows with system size. Near $p = 0$, no such trend is visible, see also the inset of Fig. 9. In particular, no clear crossing of the curves can be observed, which would be an indication that a finite fraction of inverted hard bonds is necessary to create system spanning domain walls. Thus, system-spanning domain walls exist in the thermodynamic limit also for $p = 0$, but not many.

To obtain a clearer picture, we also measure for each system the size of the largest nontrivial domain wall (the largest trivial domain contains the spins which have not changed) in units of the system size L , when projected onto the y axis. The resulting length l_{DW} averaged over disorder is displayed in Fig. 10. One can see that the domain walls grow with increasing fraction p of the inverted hard bonds. For $p = 0$ (see the inset of Fig. 10), l_{DW} seems to converge to a quite large value, larger than 0.5. This means that the periodic boundary conditions create domain walls of order system size, although not spanning the system. For these domain walls (one can call them also droplets pinned at the border) indeed a scaling of their energy proportional to L^θ can be expected. Hence, there is an intuitively clear reason for the appearance of the nontrivial scaling term, which we have found above when studying the ground-state energy of two-dimensional systems.

VIII. CONCLUSIONS

We have analyzed the size-dependent energies for two-dimensional ISGs with Gaussian and $\pm J$ interactions, up to large sizes and for three different types of boundary

conditions: free along both axes of the sample (ffbc), periodic (ppbc) and free/periodic (pfbc).

With a simple scaling expression and three free parameters, excellent fits can be obtained to the ffbc free boundary condition data, from the isolated spin $L = 1$ up to large sizes, $L = 320$ for the Gaussian and $L = 480$ for the $\pm J$ cases. The fitting parameters can be translated into bulk-, edge-, and corner-spin (or bond) energies. The bulk ground state energy per spin is $e_\infty = -1.31479(2)$ for the Gaussian and $e_\infty = -1.40197(1)$ for the $\pm J$ case. The former is considerably more accurate than previous estimates, and the latter is consistent with the high-precision published value.⁹ The effective edge and corner bond energies do not seem to have been measured before; they are more negative than the bulk values as might be expected because of geometrically reduced frustration. It is remarkable that although the entire range of L including $L = 1$ is used, three parameters only are sufficient for an excellent fit in both cases.

For the periodic-periodic boundary condition geometry, a scaling analysis of the Gaussian system data can be made using only parameters (e_∞ and the stiffness exponent θ) whose values are already accurately known. The zero free-parameter “fit” passes through $e_{L=1} = 0$ just as for the ffbc case. Thus for the Gaussian system the scaling in these two geometries appears to be excellent, implying that any correction terms present are very small.

For the $\pm J$ system, the ppbc fit is less satisfying than for the Gaussian case, as an acceptable fit requires the introduction of a correction to scaling term. Even with this supplementary term included the global fit is not as good as for the Gaussian case.

In the mixed pfbc geometry the fit to the Gaussian data needs the introduction of a weak analytic correction term, and the extrapolation to $L = 1$ does not quite go through $e_{L=1} = 0$. The scaling is thus slightly less aesthetically pleasing than for the ffbc or ppbc geometries but follows standard correction to scaling rules.

For the $\pm J$ system any fit to the pfbc data based on the same approach as for the Gaussian is very poor. In this geometry, for the size dependence of the energy as for the directly measured domain-wall stiffness, there are strong deviations from scaling that do not follow the orthodox correction to scaling behavior. As these deviations do not appear in the Gaussian case, we associate them with the degenerate ground state of the $2d \pm J$ ISG, as discussed above. This hypothesis could be checked by measurements on other $2d$ ISG systems with degenerate ground states.

By studying explicitly sample by sample the same system having ffbc and pfbc, we have seen that indeed domain walls of order of the system size are created by the periodic boundary conditions, although usually these domain walls (or pinned droplets) do not span the whole system. The appearance of these domain walls explains the occurrence of the L^θ term in the size dependence of the ground-state energy for periodic boundary conditions

in a quite natural way.

Acknowledgments

We would like to thank A. P. Young for useful comments and suggestions on a previous version of the manuscript. Parts of the simulations were performed at the Paderborn Center for Parallel Computing (Germany) and on a Beowulf Cluster at the Institut für Theoretische Physik of the Universität Magdeburg (Germany). We would like to thank the group of Professor Michael Jünger

at the University of Cologne for placing their spin-glass server (Ref. 29) in the public domain, and for not complaining when we crashed their mail server twice due to large amounts of incoming ground-state configurations. In particular we would like to thank Frauke Liers for help concerning the spin-glass server. AKH obtained financial support from the *VolkswagenStiftung* (Germany) within the program “Nachwuchsgruppen an Universitäten” and from the Institute for Scientific Interchange (ISI) Foundation in Turin via the Complex Systems Network of Excellence “Exystence.”

-
- ¹ K. Binder and A. P. Young, *Spin glasses: Experimental facts, theoretical concepts and open questions*, Rev. Mod. Phys. **58**, 801 (1986).
- ² M. Mézard, G. Parisi, and M. A. Virasoro, *Spin Glass Theory and Beyond* (World Scientific, Singapore, 1987).
- ³ K. H. Fisher and J. A. Hertz, *Spin Glasses* (Cambridge University Press, Cambridge, 1991).
- ⁴ A. P. Young, ed., *Spin Glasses and Random Fields* (World Scientific, Singapore, 1998).
- ⁵ N. Kawashima and H. Rieger, *Recent Progress in Spin Glasses* (2003), (cond-mat/0312432).
- ⁶ L. Bieche, J. P. Uhry, R. Maynard, and R. Rammal, *On the ground states of the frustration model of a spin glass by a matching method of graph theory*, J. Phys. A **13**, 2553 (1980).
- ⁷ F. Barahona, R. Maynard, R. Rammal, and J. P. Uhry, *Morphology of ground-states of two-dimensional frustration model*, J. Phys. A **15**, 673 (1982).
- ⁸ U. Derigs and A. Metz, *Solving (large scale) matching problems combinatorially*, Math. Prog. **50**, 113 (1991).
- ⁹ R. G. Palmer and J. Adler, *Ground states of large samples of two-dimensional Ising spin glasses*, Int. J. Mod. Phys. C **10**, 667 (1999).
- ¹⁰ A. K. Hartmann and A. P. Young, *Lower critical dimension of Ising spin glasses*, Phys. Rev. B **64**, 180404 (2001), (cond-mat/0107308).
- ¹¹ J.-S. W. Z.F. Zhan, L.W. Lee, *A new approach to the study of the ground-state properties of 2D Ising spin glass*, Physica A **295**, 239 (2000).
- ¹² J. Houdayer, *A cluster Monte Carlo algorithm for 2-dimensional spin glasses*, Eur. Phys. J. B. **22**, 479 (2001).
- ¹³ H. Rieger, L. Santen, U. Blasum, M. Diehl, M. Jünger, and G. Rinaldi, *The critical exponents of the two-dimensional Ising spin glass revisited: exact ground-state calculations and Monte Carlo simulations*, J. Phys. A **29**, 3939 (1996).
- ¹⁴ H. G. Katzgraber and A. P. Young, *Numerical studies of the two- and three-dimensional gauge glass at low temperature*, Phys. Rev. B **66**, 224507 (2002), (cond-mat/0205206).
- ¹⁵ H. G. Katzgraber, L. W. Lee, and A. P. Young, *Correlation Length of the Two-Dimensional Ising Spin Glass with Gaussian Interactions* (2004), (cond-mat/0402037).
- ¹⁶ J. Houdayer and A. K. Hartmann, *Low temperature behavior of two-dimensional Gaussian Ising spin glasses* (2004), (cond-mat/0402036).
- ¹⁷ C. Amoruso, E. Marinari, O. C. Martin, and A. Pagnani, *Scalings of Domain Wall Energies in Two Dimensional Ising Spin Glasses*, Phys. Rev. Lett. **91**, 87201 (2003).
- ¹⁸ L. Saul and M. Kardar, *Exact integer algorithm for the two-dimensional $\pm J$ Ising spin glass*, Phys. Rev. E **48**, R3221 (1993).
- ¹⁹ L. Saul and M. Kardar, *The 2d $\pm J$ Ising spin glass: exact partition functions in polynomial time*, Nucl. Phys. B **432**, 641 (1994).
- ²⁰ J. Lukic, A. Gallucio, E. Marinari, O. C. Martin, and G. Rinaldi, *Critical thermodynamics of the two dimensional $\pm j$ Ising spin glass* (2003), (cond-mat/0309238).
- ²¹ M. A. Moore, *Corrections to scaling in the droplet picture of spin glasses* (2002), (cond-mat/0203469).
- ²² L. Berthier and A. P. Young, *Energetics of clusters in the two dimensional Ising spin glass*, J. Phys. A **36**, 10835 (2003).
- ²³ A. K. Hartmann, A. J. Bray, A. C. Carter, M. A. Moore, and A. P. Young, *The stiffness exponent of two-dimensional Ising spin glasses for non-periodic boundary conditions using aspect-ratio scaling*, Phys. Rev. B **66**, 224401 (2002), (cond-mat/0208546).
- ²⁴ A. K. Hartmann and M. A. Moore, *Corrections to scaling are large for droplets in two-dimensional spin glasses*, Phys. Rev. Lett. **90**, 127201 (2003), (cond-mat/0210587).
- ²⁵ F. Barahona, *On the computational complexity of Ising spin glass models*, J. Phys. A **15**, 3241 (1982).
- ²⁶ A. K. Hartmann and H. Rieger, *Optimization Algorithms in Physics* (Wiley-VCH, Berlin, 2002).
- ²⁷ G. Toulouse, *Theory of the frustration effect in spin glasses*, Commun. Phys. **2**, 115 (1977).
- ²⁸ K. Mehlhorn and S. Näher, *The LEDA Platform of Combinatorial and Geometric Computing* (Cambridge University Press, Cambridge, 1999), also <http://www.mpi-sb.mpg.de/LEDA/leda.html>.
- ²⁹ Information about the spin glass ground state server at the University of Köln can be found at http://www.informatik.uni-koeln.de/l_s_juenger/projects/sg.html.
- ³⁰ C. De Simone, M. Diehl, M. Jünger, P. Mutzel, G. Reinelt, and G. Rinaldi, *Exact ground states in spin glasses: New experimental results with a branch-and-cut algorithm*, J. Stat. Phys. **80**, 487 (1995).
- ³¹ C. De Simone, M. Diehl, M. Jünger, P. Mutzel, G. Reinelt, and G. Rinaldi, *Exact Ground States of Two-Dimensional $-J$ Ising Spin Glasses*, J. Stat. Phys. **84**, 1363 (1996).
- ³² *Lecture notes in computer science 2241*, in *Computational*

- Combinatorial Optimization*, edited by M. Jünger and D. Naddef (Springer Verlag, Heidelberg, 2001).
- ³³ M. Palassini, F. Liers, M. Jünger, and A. P. Young, *Low energy excitations in spin glasses from exact ground states*, Phys. Rev. B **68**, 064413 (2003), (cond-mat/0212551).
- ³⁴ J. M. Yeomans, *Statistical mechanics of Phase transitions* (Oxford University Press, Oxford, 1992).
- ³⁵ H. G. Katzgraber and A. P. Young, *Monte Carlo simulations of spin-glasses at low temperatures: Effects of free boundary conditions*, Phys. Rev. B **65**, 214402 (2002), (cond-mat/0108544).
- ³⁶ A. J. Bray and M. A. Moore, *Lower critical dimension of Ising spin glasses: a numerical study*, J. Phys. C **17**, L463 (1984).
- ³⁷ J.-P. Bouchaud, F. Krzakala, and O. Martin, *Energy exponents and corrections to scaling in Ising spin glasses*, Phys. Rev. B **68**, 224404 (2003), (cond-mat/0212070).
- ³⁸ J. Salas and A. D. Sokal, *Universal Amplitude Ratios in the Critical Two-Dimensional Ising Model on a Torus* (1999), (cond-mat/9904038v1).
- ³⁹ J. Salas and A. D. Sokal, *Universal Amplitude Ratios in the Critical Two-Dimensional Ising Model on a Torus*, J. Stat. Phys. **98**, 551 (2000), (cond-mat/9904038).
- ⁴⁰ J. Salas, *Exact finite size scaling corrections to the critical two dimensional Ising model on a torus*, J. Phys. A **34**, 1311 (2001).
- ⁴¹ C. de Dominicis, (private communication).